Finite-difference time-domain solution of light scattering by dielectric particles with a perfectly matched layer absorbing boundary condition

Wenbo Sun, Qiang Fu, and Zhizhang Chen

A three-dimensional finite-difference time-domain (FDTD) program has been developed to provide a numerical solution for light scattering by nonspherical dielectric particles. The perfectly matched layer (PML) absorbing boundary condition (ABC) is used to truncate the computational domain. As a result of using the PML ABC, the present FDTD program requires much less computer memory and CPU time than those that use traditional truncation techniques. For spheres with particle-size parameters as large as 40, the extinction and absorption efficiencies from the present FDTD program match the Mie results closely, with differences of less than ~1%. The difference in the scattering phase function is typically smaller than ~5%. The FDTD program has also been checked by use of the exact solution for light scattering by a pair of spheres in contact. Finally, applications of the PML FDTD to hexagonal particles and to spheres aggregated into tetrahedral structures are presented.

OCIS codes: 010.1290, 010.1310, 010.3920, 290.5850, 290.1090, 280.1100.

1. Introduction

Cirrus clouds, primarily present in the upper troposphere and lower stratosphere, are globally distributed and are composed almost exclusively of nonspherical ice crystals.[1–3] Remote-sensing studies and climate research require precise knowledge of scattering and absorption by nonspherical ice crystals.[4–6] To date, however, except for some simple particle shapes,[7] such as spheres,[8] double-sphere systems,[9] spheroids,[10] infinite circular cylinders,[11,12] Chebyshev particles,[13] finite circular cylinders,[14] and cubes,[15] theoretical scattering treatments are not available for scattering and absorption by nonspherical particles. Of the ways other than analytical solutions, Rayleigh theory can be applied when the particle-size parameter is much smaller than one. When the size parameter is larger than ~40, the geometric optics method[16–18] can be used for nonspherical particles. However, in the resonant region,[19] Rayleigh theory and the geometric optics method are not applicable because of the assumptions pertaining to each technique.

It was recently suggested that the anomalous diffraction theory[20] would be an appropriate method for calculating the single-scattering properties of nonspherical ice particles.[21] However, this method is not able to provide information on the scattering phase functions. In addition, it is found that the anomalous diffraction theory presents large errors if the refractive index is not close to one.[6,22,23] Because ice presents a large range of refractive indices in both real and imaginary parts, the applicability of the anomalous diffraction theory to nonspherical ice crystals is limited.

To obtain accurate solutions for light scattering by particles of arbitrary shapes, numerical approaches such as the discrete dipole approximation[24–27] have been developed. However, it may work well only for nonspherical particles with size parameters smaller than ~15.[28,29]

Pioneered by the research of Yee[30] and many other electrical engineers, the finite-difference time-domain (FDTD) solutions of Maxwell's equations have been extensively applied to electromagnetic problems such as antenna design, radar cross-section computation, waveguide analysis, and some other open-structure problems. The FDTD technique is a

The authors are with Dalhousie University, Halifax, Nova Scotia B3H 4J1, Canada. W. Sun and Q. Fu are with the Atmospheric Science Program, Department of Oceanography; Z. Chen is with the Department of Electrical and Computer Engineering. The e-mail address for Q. Fu is qfu@atm.dal.ca.

Received 3 August 1998; revised manuscript received 6 January 1999.

0003-6935/99/153141-11$15.00/0

numerical solution to Maxwell's equations and is formulated by replacing temporal and spatial derivatives in Maxwell's equations with their finite-difference correspondences. This method can be accurately applied to general electromagnetic structures including particles of arbitrary shapes. However, like other numerical approaches, the FDTD method requires large computer storage and large CPU time even for particles with small size parameters. Moreover the stability and accuracy of the FDTD program are determined by many factors such as boundary condition, mesh size, and scatterer size. Topics related to improvement of its accuracy, reduction of memory and CPU time requirement, and applications to larger objects, have been actively pursued over the past 10 years.[31–34]

In applications of the FDTD technique to problems in an unbounded space, one of the key issues is the truncation of the computational domain through artificial boundary conditions. In the case of studying light scattering by particles of arbitrary shapes, it is essential to use the most effective and efficient boundary treatment. Yang and Liou[35] employed the FDTD method for light scattering by small nonspherical ice crystals by using a transmitting boundary condition.[36,37] They found that the FDTD works well for particles with size parameters smaller than 10. In this study we have developed a FDTD program by employing a newly developed so-called perfectly matched layer (PML) absorbing boundary condition (ABC).[38–40] We apply the FDTD program for light scattering by dielectric particles with size parameters as large as 40 to show its accuracy and efficiency. In Section 2 the FDTD with PML ABC for dielectric scatterers is formulated. In Section 3 the FDTD program is validated by using the exact solutions. Some applications of the present program to nonspherical particles are presented in Section 4. Summary and conclusions are in Section 5.

2. Finite-Difference Time-Domain Method with a Perfectly Matched Layer Absorbing Boundary Condition

A. Finite-Difference Time-Domain Method

The FDTD formulations of electromagnetic-field problems is a direct numerical solution of Maxwell's time-dependent curl equations. Consider a source-free medium where Maxwell's equations can be written as

$$\nabla \times \mathbf{E} = -\mu \frac{\partial \mathbf{H}}{\partial t}, \tag{1a}$$

$$\nabla \times \mathbf{H} = \epsilon \frac{\partial \mathbf{E}}{\partial t}, \tag{1b}$$

where $\mathbf{E}$ and $\mathbf{H}$ are the electric and the magnetic fields, respectively, μ is the permeability, and ϵ is the permittivity of the dielectric medium.

Assuming that the time-dependent part of the electromagnetic field is $\exp(-i\omega t)$, the electric and the magnetic fields can be written in the form

$$\mathbf{E}(x, y, z, t) = \mathbf{E}(x, y, z)\exp(-i\omega t), \tag{2a}$$

$$\mathbf{H}(x, y, z, t) = \mathbf{H}(x, y, z)\exp(-i\omega t), \tag{2b}$$

where $\omega = kc$, k is the wave number, and c is the speed of the electromagnetic wave in free space. ϵ is complex for an absorptive medium and can be expressed as

$$\epsilon = \epsilon_r + i\epsilon_i. \tag{3a}$$

Since refractive index $m = (\epsilon\mu)^{1/2}$ and for a nonferromagnetic medium μ is unity, the real and the imaginary parts of ϵ may be expressed by the real and the imaginary parts of m in the form

$$\epsilon_r = m_r^2 - m_i^2, \qquad \epsilon_i = 2m_r m_i. \tag{3b}$$

To apply the FDTD method for light scattering by small ice crystals, Yang and Liou[35] introduced a way of transforming Maxwell's equations to a source-dependent form that governs the scattering process of a dielectric particle so that complex calculations can be avoided when the scatterer is absorptive. Here the equivalent Maxwell's equations for an absorptive scatterer are derived without introducing the effective current as Yang and Liou[35] did.

Inserting Eqs. (2) into Eq. (1b) and using Eq. (3a), we have

$$\nabla \times \mathbf{H}(x, y, z) = \omega(\epsilon_i - i\epsilon_r)\mathbf{E}(x, y, z). \tag{4}$$

Multiplying Eq. (4) with $\exp(-i\omega t)$ and using Eqs. (2) and (3a), we obtain

$$\nabla \times \mathbf{H}(x, y, z, t) = \omega\epsilon_i \mathbf{E}(x, y, z, t) + \epsilon_r \frac{\partial \mathbf{E}(x, y, z, t)}{\partial t}. \tag{5}$$

Equation (5) can be further simplified to

$$\frac{\partial[\exp(\tau t)\mathbf{E}(x, y, z, t)]}{\partial t} = \frac{\exp(\tau t)}{\epsilon_r} \nabla \times \mathbf{H}(x, y, z, t), \tag{6}$$

where $\tau = \omega\epsilon_i/\epsilon_r$. Using the central finite-difference approximation for the temporal derivative in Eq. (6) over the time interval $[n\Delta t, (n + 1)\Delta t]$, we have

$$\mathbf{E}^{n+1}(x, y, z) = \exp(-\tau\Delta t)\mathbf{E}^n(x, y, z) + \exp(-\tau\Delta t/2) \frac{\Delta t}{\epsilon_r} \nabla \times \mathbf{H}^{n+1/2}(x, y, z), \tag{7a}$$

where the electric and the magnetic fields are evaluated at alternating half-time steps.[30]

By discretizing Eq. (1a) over the time interval of $[(n - 1/2)\Delta t, (n + 1/2)\Delta t]$, which is a half-time step

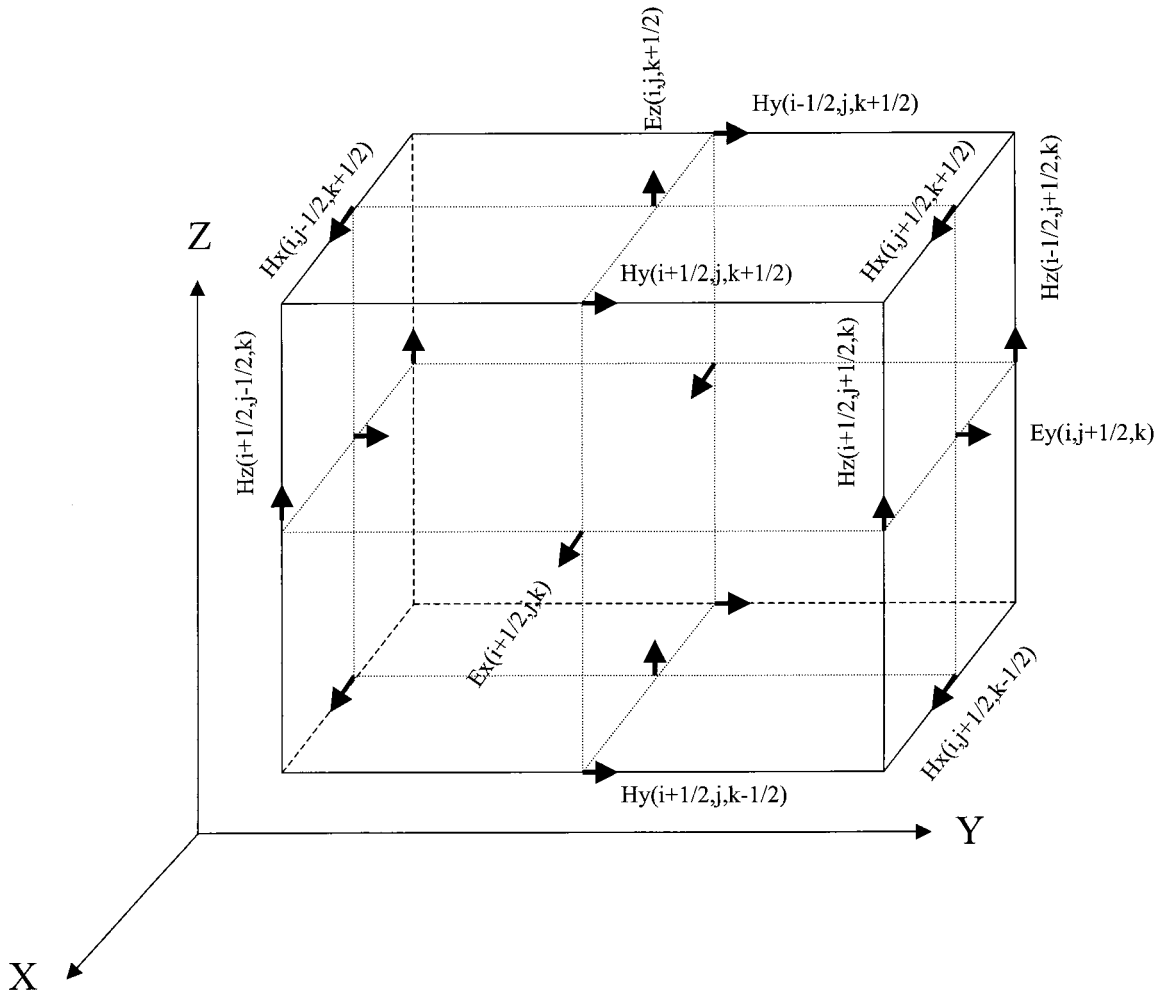

Fig. 1. Positions of the electric- and the magnetic-field components in an elementary cubic cell of the FDTD lattice.

earlier than the time step when the electric field is evaluated, we have

$$\mathbf{H}^{n+1/2}(x, y, z) = \mathbf{H}^{n-1/2}(x, y, z) - \frac{\Delta t}{\mu} \nabla \times \mathbf{E}^{n}(x, y, z). \tag{7b}$$

In Eqs. (7a) and (7b), Δt is the time increment and n is an integer denoting the time step.

Let $\delta = \Delta x = \Delta y = \Delta z$ denote the space increment; the explicit finite-difference approximation of Eq. (7) can be derived in the following forms:

$$\begin{aligned} H_x^{n+1/2}(i, j + 1/2, k + 1/2) = {} & H_x^{n-1/2}(i, j \\ & + 1/2, k + 1/2) \\ & + \frac{\Delta t}{\mu(i, j + 1/2, k + 1/2)\delta} \\ & \times [E_y^{n}(i, j + 1/2, k + 1) \\ & - E_y^{n}(i, j + 1/2, k) \\ & + E_z^{n}(i, j, k + 1/2) \\ & - E_z^{n}(i, j + 1, k + 1/2)], \end{aligned} \tag{8a}$$

$$\begin{aligned} E_x^{n+1}(i + 1/2, j, k) = {} & \exp[-\tau(i + 1/2, j, k)\Delta t] \\ & \times E_x^{n}(i + 1/2, j, k) \\ & + \exp[-\tau(i \\ & + 1/2, j, k)\Delta t/2] \\ & \times \frac{\Delta t}{\epsilon_r(i + 1/2, j, k)\delta} \\ & \times [H_z^{n+1/2}(i + 1/2, j \\ & + 1/2, k) - H_z^{n+1/2}(i \\ & + 1/2, j - 1/2, k) \\ & + H_y^{n+1/2}(i + 1/2, j, k \\ & - 1/2) - H_y^{n+1/2}(i \\ & + 1/2, j, k + 1/2)]. \end{aligned} \tag{8b}$$

The positions of the field components are illustrated in Fig. 1.

To obtain accurate numerical results, the spatial increment δ must be much smaller than the wavelength within the scatterer and its minimum di-

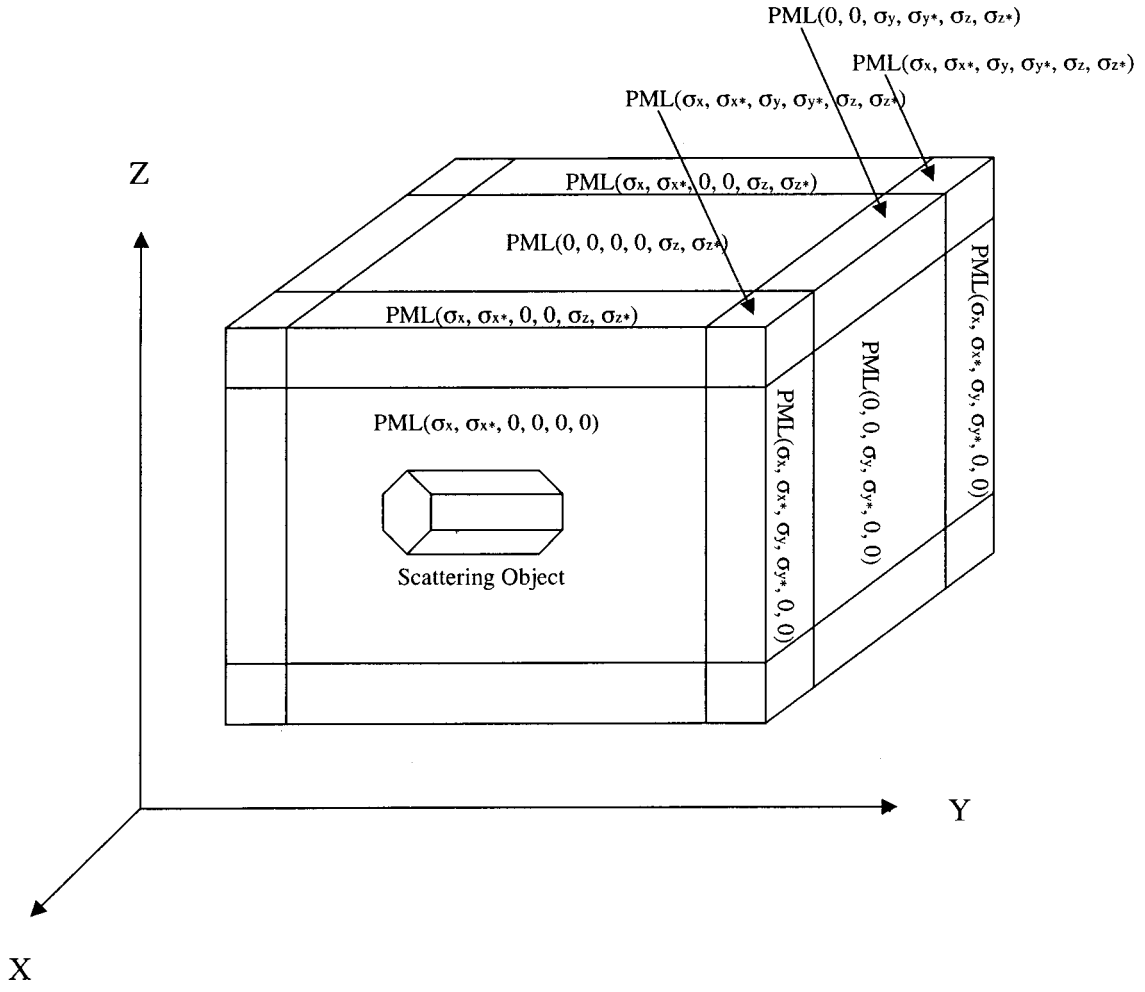

Fig. 2. Computational domain terminated by the PML. The arrangement of the fictitious electric conductivity (σ) and magnetic conductivity (σ^*) in the PML walls is also shown.

mension. To guarantee the stability of the FDTD computation, the time increment Δt must satisfy the following condition[41]:

$$c\Delta t \leq \left(\frac{1}{\Delta x^2} + \frac{1}{\Delta y^2} + \frac{1}{\Delta z^2}\right)^{-1/2}, \tag{9}$$

where c is the wave velocity within the scatterer.

The near fields are computed in the time domain. To calculate the single-scattering properties of the dielectric scatterer, the time-dependent fields obtained must be transformed to the corresponding fields in the frequency domain.[35] In this study the discrete Fourier transform is used throughout the time-marching steps to get the fields in the frequency domain from the time series.

B. Perfectly Matched Layer Absorbing Boundary Condition

One major difficulty encountered in applying the FDTD method to the open-structure problem is that the domain where the field is computed is unbounded. Since a finite-difference scheme over an infinite domain is impractical, the extent of the solution region must be limited by using an artificial ABC.[42] The accuracy and stability of the FDTD program would be sensitive to the boundary condition used. Early approaches for the boundary condition are mostly one-way wave-equation approximation techniques.[43] Among those are Mur's second- and third-order ABC,[44] outgoing-wave annihilators,[45] transmitting boundary conditions,[36] and the Higdon method.[46] A recent development in ABC's was the PML ABC.[38–40] In the two-dimensional case,[38] it is reported that the reflection coefficients of the PML are as low as 1/3000th of those based on standard second- and third-order analytical ABC's. The PML for the three-dimensional case[40] works as well as in the two-dimensional case.

To apply the FDTD method with PML ABC to a three-dimensional light-scattering problem, the original finite-difference algorithm developed by Yee[30] needs to be modified. Following Berenger[39] and Katz *et al.*,[40] the normal FDTD computational space is surrounded by PML regions as shown in Fig. 2, backed up by perfectly conducting walls. The PML creates a fictitious absorbing layer adjacent to the outer grid boundary. In the inner volume the finite-

difference equations are the usual discretizations of Maxwell's equations. In the PML regions six Cartesian components of electric and magnetic vectors are split into 12 (e.g., H_x is split into H_{xy} and H_{xz}, and E_x is split into E_{xy} and E_{xz}), resulting in 12 modified Maxwell's equations, such as

$$\mu_0 \frac{\partial H_{xy}}{\partial t} + \sigma_y^* H_{xy} = -\frac{\partial (E_{zx} + E_{zy})}{\partial y}, \tag{10a}$$

$$\mu_0 \frac{\partial H_{xz}}{\partial t} + \sigma_z^* H_{xz} = \frac{\partial (E_{yx} + E_{yz})}{\partial z}, \tag{10b}$$

$$\epsilon_0 \frac{\partial E_{xy}}{\partial t} + \sigma_y E_{xy} = \frac{\partial (H_{zx} + H_{zy})}{\partial y}, \tag{10c}$$

$$\epsilon_0 \frac{\partial E_{xz}}{\partial t} + \sigma_z E_{xz} = -\frac{\partial (H_{yx} + H_{yz})}{\partial z}, \tag{10d}$$

where the subscript 0 denotes the vacuum medium and σ and σ^* are the fictitious electric and magnetic conductivities, respectively, which satisfy

$$\frac{\sigma}{\epsilon_0} = \frac{\sigma^*}{\mu_0}. \tag{11}$$

Equation (11) allows the impedance of the fictitious medium equal to that of free space, and thus no reflection occurs when a plane wave propagates across a vacuum–PML interface.

On the six sides of the PML regions the absorbing PML layers are matched to each other by having transverse conductivities equal to zero. As a result the outgoing waves from the inner vacuum would propagate into these absorbing layers without reflection. At the 12 edges two conductivities are equal to zero but the other four are equal to those of the adjacent side PML's. Thus there is also no reflection from the side–edge interfaces. In the eight corners of the PML the conductivities are assigned to those of the adjacent edges; all of the 12 conductivities are not zero. Therefore the reflection equals zero from all the edge–corner interfaces. The arrangement of fictitious conductivities in the PML is shown in Fig. 2. In theory only the ideal continuous PML media can have a perfect match without reflections. In the numerical PML, owing to step-type variations of conductivities between the PML sublayers and the break in the fields, a certain amount of numerical reflection and dispersion would occur. To reduce this reflection and dispersion, the conductivities should increase smoothly from a small value on the vacuum–PML interfaces to a large value on the outer boundaries. Thus, to approximate a continuous media, the number of PML cells used should be sufficient to approximate a continuous media.

After crossing the PML layer, the wave is reflected by the perfectly conducting conditions that end the PML region, and then, after a second crossing, it can come back into the normal FDTD computational space. So, for a PML layer of thickness d, an apparent reflection factor is found to be

$$R(\theta) = \exp\left[-\frac{2\cos\theta}{\epsilon_0 c}\int_0^d \sigma(\rho)\mathrm{d}\rho\right], \tag{12}$$

where θ is the angle of incident radiation relative to the normal direction of the PML surface.

Berenger[38] proposes that the conductivities should increase with depth within PML as

$$\sigma(\rho) = \sigma_m\left(\frac{\rho}{d}\right)^n, \tag{13}$$

where n can be 1, 2, 3, etc. but unnecessarily an integer. In this study we set $n = 3$. From Eqs. (12) and (13) the apparent reflection can be expressed as

$$R(\theta) = [R(0)]^{\cos(\theta)}, \tag{14}$$

where $R(0)$ is the reflection factor at normal incidence. $R(0)$ is a key user-defined parameter that can be expressed as

$$R(0) = \exp\left(-\frac{2}{n+1}\frac{\sigma_m d}{\epsilon_0 c}\right). \tag{15}$$

For grazing incidence θ is close to $\pi/2$, and then the factor $R(\theta)$ is close to unity with any given σ. So the grazing incidence may cause some numerical reflections. Therefore the scatterer and the PML should not be too close so that there will not be scattered waves impinging on the PML at grazing angles. Furthermore Eq. (15) suggests that the PML should have sufficient thickness, or a sufficient number of cells, to achieve small reflections, which is another important reason why the number of PML layers should be kept at a reasonable level.

The PML scheme has been successfully extended to the transmission-line-method-based FDTD method[31] and for the absorption of nonlinear electromagnetic waves.[32] The reflection factor has been found to be better than 10^{-6} with 16 PML layers even in nonlinear cases.

C. Wave Source

We implement, based on the equivalence theorem,[47,48] a plane-wave source by using the closed surface of a rectangular box within the vacuum region of the computational domain. The equivalence theorem states that the existence of a wave-excitation source can be replaced by the equivalent electric and magnetic currents on a closed surface for the spatial domain inside the surface. If there is a scatterer inside this closed surface, the interior fields will be the total fields (incident and scattered) and the fields outside are just the scattered fields. On the closed surface both electric and magnetic sources are added to the fields as

$$\mathbf{H} \leftarrow \mathbf{H} - \frac{\Delta t}{\mu_0 \Delta s}(\mathbf{E}^{\mathrm{in}} \times \mathbf{n}), \tag{16a}$$

$$\mathbf{E} \leftarrow \mathbf{E} - \frac{\Delta t}{\epsilon_0 \Delta s}(\mathbf{n} \times \mathbf{H}^{\mathrm{in}}), \tag{16b}$$

where $\mathbf{H}^{in}$ and $\mathbf{E}^{in}$ are the incident fields, $\mathbf{n}$ is the inward normal vector of the closed surface, and $\Delta s = \delta$. For numerical implementation, note that the nodes of $\mathbf{E}$ and $\mathbf{H}$ are at different spatial grid points. Furthermore $\mathbf{H}^{in}$ and $\mathbf{E}^{in}$ may come from arbitrary directions. Therefore light scattering by an arbitrarily oriented particle can be computed.

Herein a Gaussian pulse is used as a plane-wave source in the form

$$E(t) = \exp\left[-\left(\frac{t}{30\Delta t} - 5\right)^2\right]. \quad (17)$$

3. Validation of the Perfectly Matched Layer Finite-Difference Time Domain

In principle the FDTD method can be accurately applied to particles of arbitrary shape. However, there are numerical errors involved in the FDTD technique. These errors can be attributed to the numerical dispersion of the finite-difference analog, the approximation of a specific particle shape by a pseudostructure constructed by cubic grid cells, the representation of the near field by the discretized data that do not account for the field variation within each cell, and reflections from the PML ABC. These errors are dependent on the grid size, the cell number in the free space between the scatterer and the PML, the cell number in the PML, etc. Yang and Liou[35] pointed out that the errors in the FDTD technique can also be attributed to the residual energy inside the computational domain when the time-marching iteration of the near field based on the pulse technique is terminated.

Throughout this paper, we set a $R(0)$ of 10^{-5} and used a six-cell PML and kept seven cells for free space between the scatterer and the PML. The sensitivity study for these parameters was reported in the study by Sun.[22] It was found that when PML ABC is used, the computational domain is reduced significantly when compared with traditional ABC approaches. In this study the computations were performed on a SunSparc workstation and Cray J90 machine for particles with size parameters of ≤ 20 and >20, respectively. In the following the PML FDTD scheme for scattering by dielectric particles is examined by use of Mie theory for spheres and the exact scattering solution for a pair of spheres in contact.

Figure 3 shows the extinction efficiency Qe, the absorption efficiency Qa, and the asymmetry factor g of spherical ice crystals computed by Mie theory and the PML FDTD method at a wavelength of 10.8 μm ($m = 1.0891 + 0.18216i$), which is a particularly important wavelength in satellite remote sensing. Also shown are the absolute and the relative errors of the PML FDTD results. In the FDTD calculations a grid size of $\Delta s = \lambda/20$ is used. We can see that the FDTD errors for both extinction efficiency and absorption efficiency are very small. For a size parameter larger than 2.0, the relative errors for Qe are within ~1.0% and the relative errors for Qa are within ~0.5%. The errors in asymmetry factors due to the FDTD are ~0.1%. These results are true even when the size parameter reaches 40. In consideration of the trend of the error, it is safe to believe that the PML FDTD can produce Qe and Qa with errors within ~1.0% for quite large size parameters. For a size parameter smaller than 2.0, the relative errors become larger for Qe, Qa, and g, because, when $\Delta s = \lambda/20$ is used, the sphere is approximated by only a few cubic cells (e.g., for a size parameter equal to 1.0, it must have only approximately six cubic cells in diameter to approach a sphere). Numerical results show that using a smaller cell size would result in more accurate results.

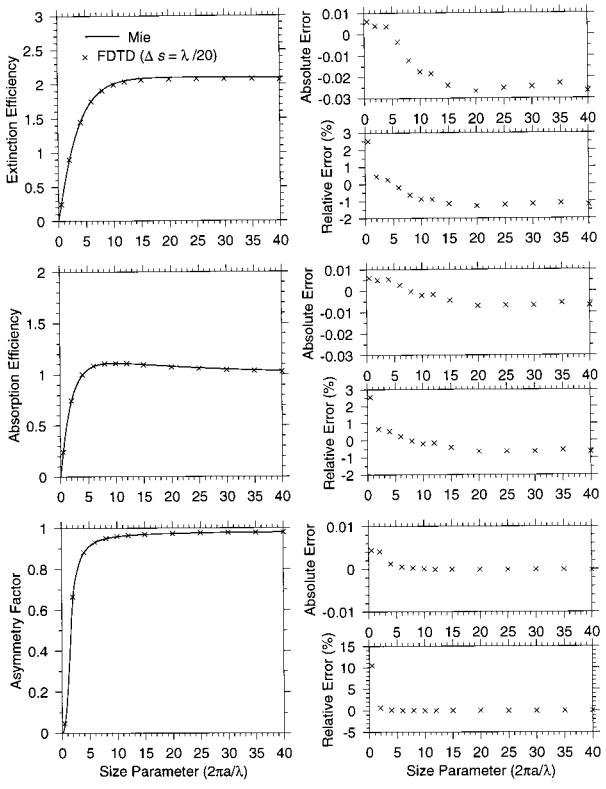

Fig. 3. Extinction efficiency, absorption efficiency, and asymmetry factor for spherical ice crystals as functions of the size parameter, $2\pi a/\lambda$, where a is the radius of the sphere and λ is the wavelength. These results are computed by Mie theory and the PML FDTD method at a wavelength of 10.8 μm ($m = 1.0891 + 0.18216i$). Also shown are the absolute and the relative errors of the FDTD results. A grid size of $\Delta s = \lambda/20$ is used in the FDTD calculation.

Noted that when $\Delta s = \lambda/20$ is used, errors due to the FDTD with the conventional boundary condition are ~5% for the extinction and the absorption efficiencies at a size parameter of 10, as reported in Fig. 5 of Yang and Liou.[35] Their errors also increased as the size parameter increased. It may be concluded that the accuracy of the FDTD method is sensitive to the boundary conditions used.

Figures 4–6 show the scattering phase functions for spherical ice crystals computed by Mie theory and the PML FDTD scheme using a wavelength of 10.8 μm for different size parameters. Also shown are

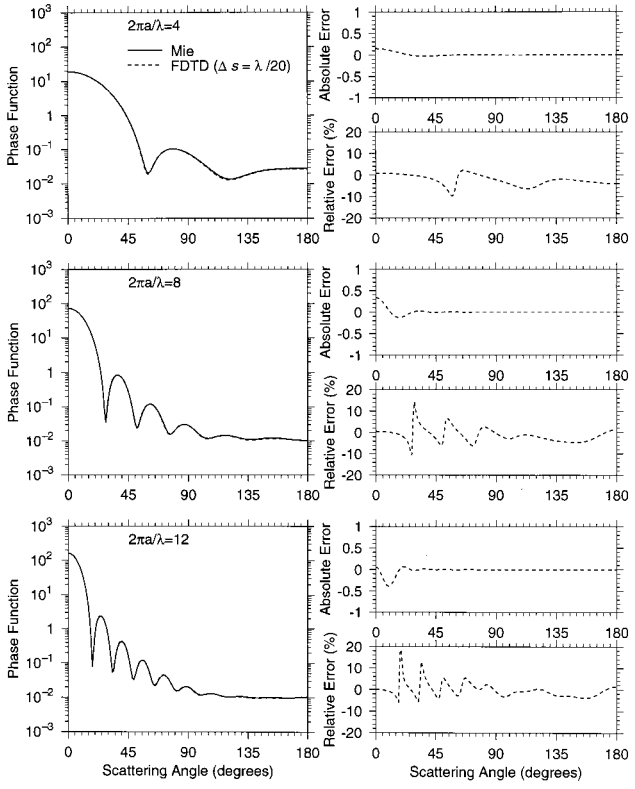

Fig. 4. Scattering phase functions for spherical ice crystals computed by Mie theory and the PML FDTD method at a wavelength of 10.8 μm ($m = 1.0891 + 0.18216i$) for different size parameters. Also shown are the absolute and the relative errors of the FDTD results. In the FDTD calculations a cell size of $\Delta s = \lambda/20$ is used.

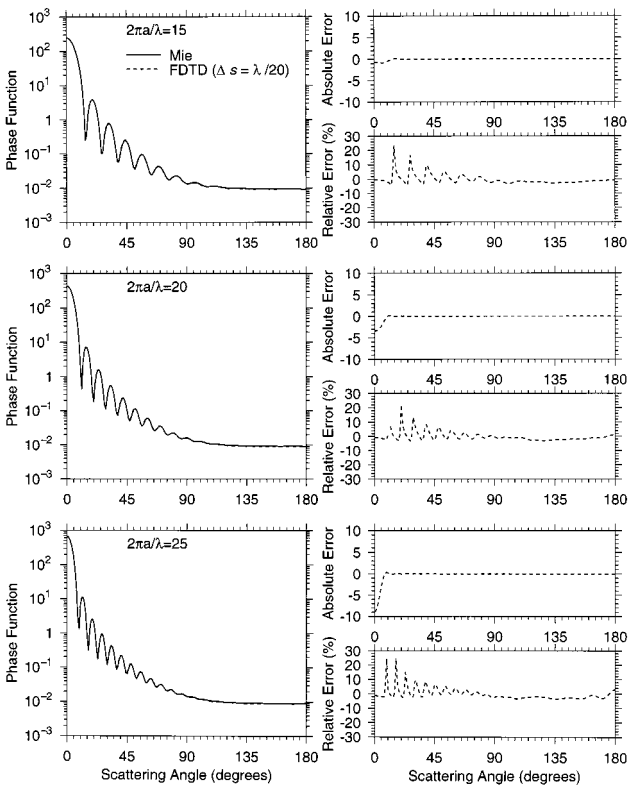

Fig. 5. Same as Fig. 4 but for size parameters of 15, 20, and 25.

the absolute and the relative errors of the FDTD results. We can see that the errors in the scattering phase functions are typically smaller than 5%. Larger errors due to the FDTD occur only when the scattering phase functions are minimum. These errors can be largely related to the numerical dispersion of the finite-difference analog and the approximation of a sphere by cubic grid cells as well as the representation of the near field by the discretized data. To reduce the errors, finer cells should be used but larger CPU time and storage space are required.

Figure 7 shows the scattering phase functions for spherical ice crystals computed by Mie theory and the PML FDTD method at wavelengths of 0.55 μm ($m = 1.311$), 10.8 μm ($m = 1.0891 + 0.18216i$), and 12.99 μm ($m = 1.4717 + 0.3890i$) for a size parameter of 6. We chose the three wavelengths to demonstrate the effectiveness of the PML FDTD for a wide range of refractive indices. In the PML FDTD calculation we used three different cell sizes of $\lambda/20$, $\lambda/30$, and $\lambda/60$ to show the effect of using smaller cells on the accuracy. Also shown are the absolute and the relative errors of phase functions computed by the PML FDTD. For a different refractive index we cannot see a significant difference in errors. Figure 7 shows that the PML FDTD program is insensitive to the refractive index or the wavelength in our application.

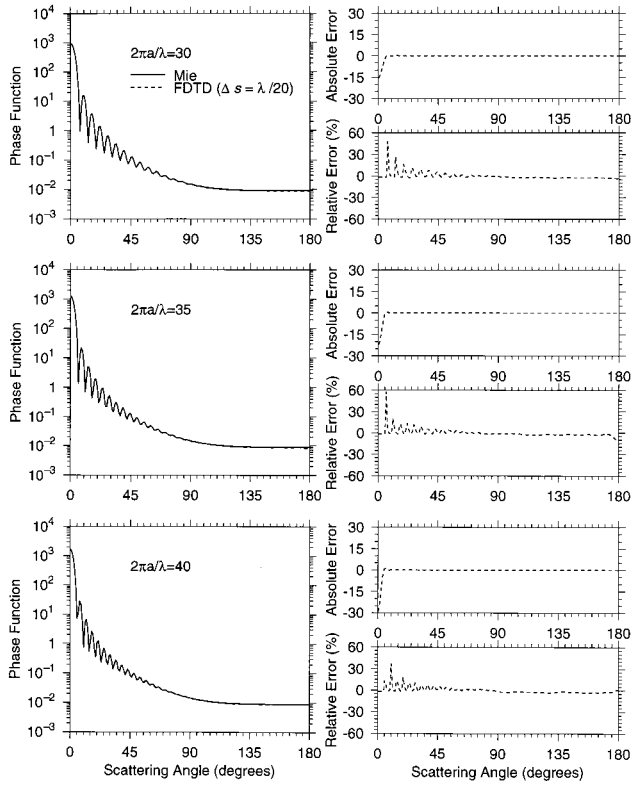

Fig. 6. Same as Fig. 4 but for size parameters of 30, 35, and 40.

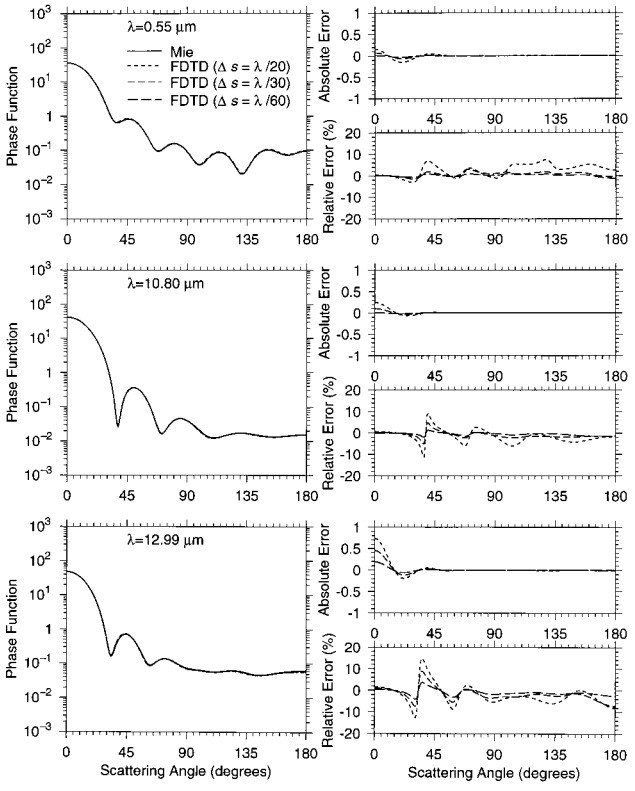

Fig. 7. Scattering phase functions for spherical ice crystals computed by Mie theory and the PML FDTD method at wavelengths of 0.55 μm ($m = 1.311$), 10.8 μm ($m = 1.0891 + 0.18216i$), and 12.99 μm ($m = 1.4717 + 0.3890i$) for a size parameter of 6. Also shown are the absolute and the relative errors of the FDTD results. Different cell sizes of $\Delta s = \lambda/20$, $\lambda/30$, and $\lambda/60$ are used in the FDTD calculations.

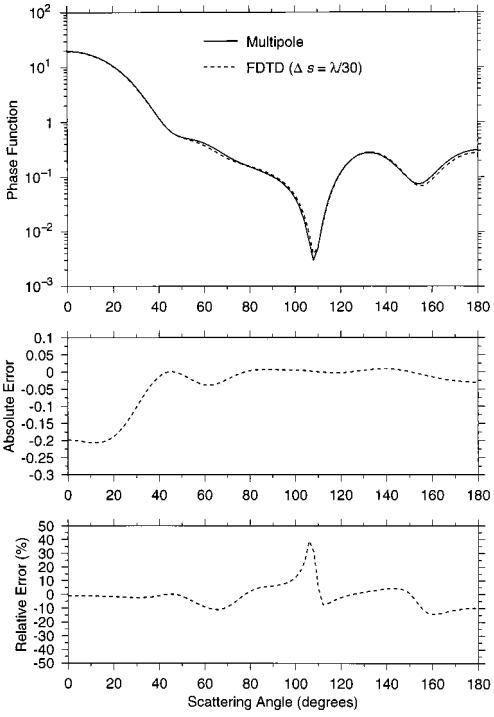

Fig. 8. Scattering phase function for a pair of spheres ($r = \lambda/2$) in contact, illuminated end-on. The results are calculated using the multipole method and the PML FDTD program with a cell size of $\Delta s = \lambda/30$; $m = 1.53 + 0.001i$ is used to represent the refractive index of biological spores at a wavelength of 0.55 μm. Also shown are the absolute and the relative errors of the FDTD results.

We can also see that the relative errors decrease when higher-resolution meshes are used for each wavelength. When $\Delta s = \lambda/60$ is used, the relative errors in the scattering phase function are smaller than ~4%.

The exact solution of light scattering by a double-sphere system is available with the multipole method.[9] Figure 8 shows a comparison of the scattering phase functions from a pair of spheres ($r = \lambda/2$ for each sphere) in contact, illuminated end-on. The PML FDTD program was used with a cell size of $\Delta s = \lambda/30$; $m = 1.53 + 0.001i$ was used to approach the refractive index of biological spores[49] at a wavelength of 0.55 μm. For this nonspherical double-sphere system, only a small discrepancy exists between the calculated results of the two models. Therefore the PML FDTD is shown to work well for nonspherical particles as well as for spherical particles.

4. Applications to Nonspherical Particles

A. Hexagonal Ice Crystals

From *in situ* aircraft observations, it has been known that cirrus clouds are largely composed of nonspherical plates, columns, and bullet rosettes[50] with a basic hexagonal structure. The size parameter for these ice crystals can range from $\sim 10^{-1}$ to 10^3 at thermal IR wavelengths (~4–100 μm). This wide size-parameter range introduces tremendous difficulty in the modeling of optical properties of nonspherical ice crystals.[28]

In both climate and remote-sensing applications, calculations involving scattering and absorption by nonspherical ice crystals at thermal IR wavelengths are usually highly simplified. Mie theory is often used but nonspherical particles must be converted first into spheres.[51,52] Other commonly used approximations include the anomalous diffraction theory[53] (ADT) and the geometric optics method[16] (GOM). For example, Sun and Shine[54] applied the GOM for hexagonal ice crystals with size parameters of greater than 30 and Mie theory for size parameters of less than 30.

Figure 9 shows the absorption efficiency of randomly oriented hexagonal ice crystals as a function of the size parameter at a wavelength of 12.99 μm ($m = 1.4717 + 0.3890i$). The aspect ratios (length/width) for these nonspherical ice crystals roughly follow observations reported by Ono[55] and Auer and Veal.[56] The results are derived from different scattering algorithms: Mie theory for a sphere using an equivalent projected area, the ADT, the GOM, and the FDTD technique. In Fig. 9 we see that in the resonant region Mie theory overestimates the absorption efficiency whereas the ADT and the GOM underesti-

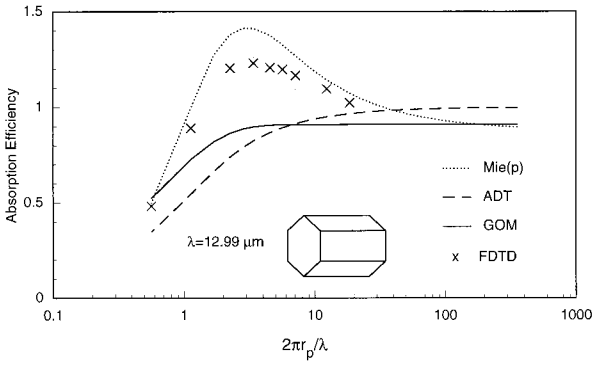

Fig. 9. Comparison of absorption efficiency for randomly oriented hexagonal ice crystals derived from a different scattering program: Mie theory for spheres with an equal projected area, ADT, a GOM, and a FDTD technique. The results are shown as functions of size parameter, $2\pi r_p/\lambda$, where r_p is the radius for a projected area equivalent sphere.

mate it. The absorption efficiency from the ADT approaches one for large size parameters because the ADT does not consider the external reflection. Differences between the ADT and the GOM for small size parameters can be explained by the absence of refraction and reflection in the ADT.

Using the single-scattering properties of hexagonal ice crystals derived from the GOM for large size parameters and the FDTD technique for small size parameters, we[6,23] have developed a composite scheme that appropriately interpolates results for size parameters between ~10 and ~50. Applying this composite technique, we examined errors in the broadband emissivity of cirrus clouds associated with conventional approaches.[6] It was found that the relative errors due to Mie theory, the ADT, and the GOM can be as large as ~30%. We have developed an accurate parameterization of the IR radiative properties of cirrus clouds for climate models by using the single-scattering properties from the composite method.[23]

B. Irregular Tetrahedral Aggregates

One type of nonspherical particle whose optical properties are of interest is the cluster of biowarfare agent spores. When a liquid solution containing such spores is aerosolized and the liquid evaporates, the compact, nearly spherical clusters of these spores remain. Early warning systems depend on rapid identification of these particles, and elastic and fluorescent light scattering may play a crucial role in the development of such systems.[57]

Herein the PML FDTD is applied to an aggregation of spores that is approximated by four spherules in a tetrahedral orientation as shown in Fig. 10. The log of the scattering intensity as a function of the zenith and the azimuthal angle for the tetrahedral structure is shown in Fig. 11 for an incident angle of 0° (z direction). We can see the enhancement at three azimuthal angles of 60°, 180°, and 300° when the zenith angle is ~40°. More discussions on the application of the PML FDTD method to light scattering from irregular tetrahedral aggregates are reported by Videen *et al.*[58]

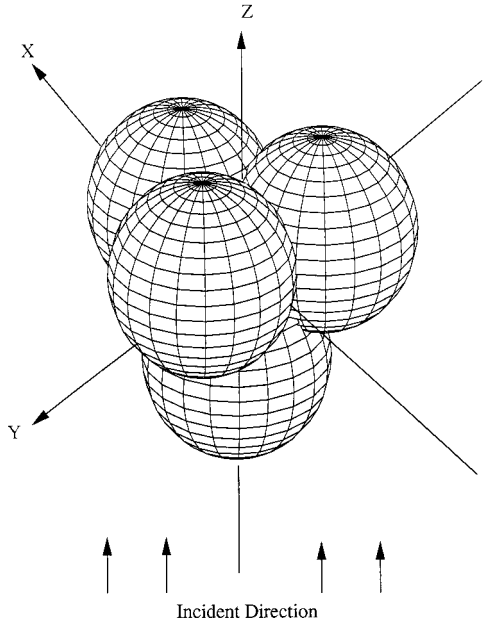

Fig. 10. Diagram of the tetrahedral scattering system. Four $r = \lambda/2$, $m = 1.53 + 0.001i$ spheres are in contact.

5. Summary and Conclusions

A finite-difference time domain (FDTD) program has been developed in this study to obtain an accurate solution of light scattering by nonspherical particles. The perfectly matched layer (PML) absorbing boundary condition (ABC) has been used. This PML FDTD program is validated by Mie theory for spheres and by the multipole method for a nonspherical double-sphere system. Compared with these reference results, the relative errors in absorption and extinction efficiencies due to the PML FDTD are

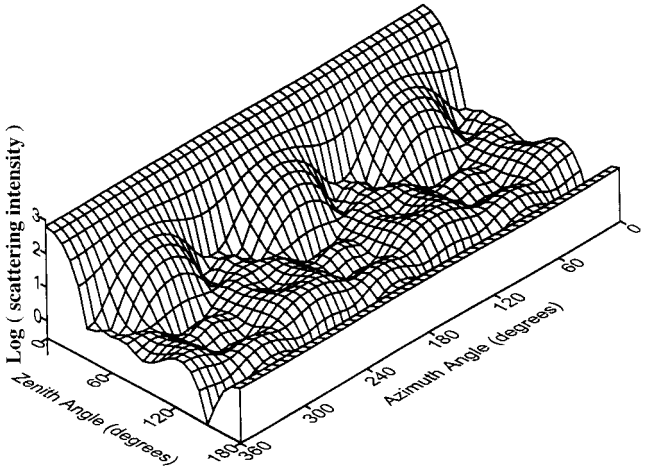

Fig. 11. Angular dependence of the scattering intensity of the system illustrated in Fig. 10 when the light is incident in the positive z direction.

within ~1% for particles with size parameters as large as 40. The relative errors for the scattering phase function are typically within ~5%. The accuracy of this technique guarantees its reliability in applications to remote-sensing and climate studies.

The PML FDTD scheme has been applied to hexagonal ice crystals at IR wavelengths. It is shown that conventional approaches to light scattering by nonspherical particles introduce significant errors, especially in the resonant region. This scheme has also been applied to light scattering by irregular tetrahedral aggregates, which has potential application to early warning systems to identify clusters of biowarfare agent spores.

Because of the use of the PML ABC, the computational domain for the FDTD is reduced significantly. In this study the computations were performed on a regular workstation even for particles with size parameters as large as 20.

The authors thank P. Chylek, G. Videen, P. Yang, and P. C. Wang for useful discussions. The research contained herein was supported by U.S. Department of Energy (DOE) grant DE-FG02-97ER62363 and in part by a Natural Sciences and Engineering Research Council (NSERC) of Canada operating grant and an Atmospheric Environment Services (Canada) (AES) science subvention grant. Part of the numerical simulations were performed on the Cray J90 computer at the National Energy Research Scientific Computing Center (NERSC). The authors thank M. Baddourah for his help with the NERSC machines.

References

1. K. N. Liou, "Influence of cirrus clouds on weather and climate processes: a global perspective," Mon. Weather Rev. **114,** 1167–1199 (1986).
2. D. O. Starr, "A cirrus cloud experiment: intensive field observations planned for FIRE," Bull. Am. Meteorol. Soc. **68,** 119–124 (1987).
3. L. M. Miloshevich, A. J. Heymsfield, and P. M. Norris, "Microphysical measurements in cirrus clouds from ice crystal replicator sonders launched during FIRE II," in *Proceedings of the 11th International Conference on Clouds and Precipitation* (Elsevier, New York, 1992), pp. 525–528.
4. G. L. Stephens, S. C. Tsay, P. W. Stackhouse, Jr., and P. J. Flatau, "The relevance of the microphysical and radiative properties of cirrus clouds to climate and climate feedback," J. Atmos. Sci. **47,** 1742–1753 (1990).
5. Y. Takano, K. N. Liou, and P. Minnis, "The effects of small ice crystals on cirrus infrared radiative properties," J. Atmos. Sci. **49,** 1487–1493 (1992).
6. Q. Fu, W. B. Sun, and P. Yang, "On modeling of scattering and absorption by nonspherical cirrus ice particles at thermal infrared wavelengths," J. Atmos. Sci. (to be published).
7. M. I. Mishchenko, L. D. Travis, and D. W. Mackowski, "T-matrix computations of light scattering by nonspherical particles. A review," J. Quant. Spectrosc. Radiat. Transfer **55,** 535–575 (1996).
8. G. Mie, "Beigrade zur optik truber medien, speziell kolloidaler metallosungen," Ann. Phys. (Leipzig) **25,** 377–445 (1908).
9. G. Videen, D. Ngo, and M. B. Hart, "Light scattering from a pair of conducting, osculating spheres," Opt. Commun. **125,** 275–287 (1996).
10. S. Asano and G. Yamamoto, "Light scattering by a spheroidal particle," Appl. Opt. **14,** 29–49 (1975).
11. J. R. Wait, "Scattering of a plane wave from a circular dielectric cylinder at oblique incidence," Can. J. Phys. **33,** 189–195 (1955).
12. Lord Rayleigh, "The dispersal of light by a dielectric cylinder," Philos. Mag. **36,** 365–376 (1918).
13. A. Mugnai and W. J. Wiscombe, "Scattering from nonspherical Chebyshev particles," Appl. Opt. **25,** 1235–1244 (1986).
14. M. I. Mishchenko, L. D. Travis, and A. Macke, "Scattering of light by polydisperse, randomly oriented, finite circular cylinders," Appl. Opt. **35,** 4927–4940 (1996).
15. H. Laitinen and K. Lumme, "T-matrix method for general star-shaped particles: first results," J. Quant. Spectrosc. Radiat. Transfer **60,** 325–334 (1998).
16. Y. Takano and K. N. Liou, "Solar radiative transfer in cirrus clouds. Part I: single-scattering and optical properties of hexagonal ice crystals," J. Atmos. Sci. **46,** 3–19 (1989).
17. P. Yang and K. N. Liou, "Geometric-optics integral-equation method for light scattering by nonspherical ice crystals," Appl. Opt. **35,** 6568–6584 (1996).
18. A. Macke, J. Muller, and E. Raschke, "Single scattering properties of atmospheric ice crystals," J. Atmos. Sci. **53,** 2813–2825 (1996).
19. P. Barber and C. Yeh, "Scattering of electromagnetic waves by arbitrarily shaped dielectric bodies," Appl. Opt. **14,** 2864–2872 (1975).
20. H. C. van de Hulst, *Light Scattering by Small Particles* (Wiley, New York, 1957).
21. D. L. Mitchell, "How appropriate is Mie theory for predicting the radiative properties of atmospheric particles?" GEWEX News 7–11 (February 1995).
22. W. B. Sun, "An investigation of infrared radiative properties of cirrus clouds," M.S. thesis (Dalhousie University, Halifax, N.S., 1997).
23. Q. Fu, P. Yang, and W. B. Sun, "An accurate parameterization of the infrared radiative properties of cirrus clouds for climate models," J. Climate **11,** 2223–2236 (1998).
24. E. M. Purcell and C. P. Pennypacker, "Scattering and absorption of light by nonspherical dielectric grains," Astrophys. J. **196,** 705–714 (1973).
25. S. B. Singham and C. F. Bohren, "Light scattering by an arbitrary particle: a physical reformation of the coupled dipole method," Opt. Lett. **12,** 10–12 (1987).
26. B. T. Draine, "The discrete-dipole approximation and its application to interstellar graphite grains," Astrophys. J. **333,** 848–872 (1988).
27. P. J. Flatau, G. L. Stephens, and B. T. Draine, "Light scattering by rectangular solids in the discrete-dipole approximation: a new algorithm exploiting the block-toeplitz structure," J. Opt. Soc. Am. A **7,** 593–600 (1990).
28. K. N. Liou and Y. Takano, "Light scattering by nonspherical particles: remote sensing and climatic implications," Atmos. Res. **31,** 271–298 (1994).
29. B. T. Draine, "The discrete dipole approximation for studying light scattering by irregular targets," in *Proceedings of Conference on Light Scattering by Nonspherical Particles* (American Meteorological Society, Boston, 1998).
30. K. S. Yee, "Numerical solution of initial boundary value problems involving Maxwell's equation in isotropic media," IEEE Trans. Antennas Propag. **AP-14,** 302–307 (1966).
31. J. Xu, Z. Chen, and J. Chuang, "Numerical implementation of PML in the TLM-based finite-difference time-domain grids," IEEE Trans. Microwave Theory Tech. **45,** 1263–1266 (1997).
32. J. Xu, J. G. Ma, and Z. Chen, "Numerical validations of a nonlinear PML scheme for absorption of nonlinear electromag-

netic waves," IEEE Trans. Microwave Theory Tech. **46,** 1752–1758 (1998).
33. C. E. Reuter, R. M. Joseph, E. T. Thiele, D. S. Katz, and T. Tflove, "Ultrawide-band absorbing boundary condition for termination of wave guide structures in FD-TD simulations," IEEE Microwave Guided Wave Lett. **4,** 344–346 (1994).
34. R. Holland, "Finite-difference time domain (FDTD) analysis of magnetic diffusion," IEEE Trans. Electromagn. Compat. **36,** 32–39 (1994).
35. P. Yang and K. N. Liou, "Finite-difference time domain method for light scattering by small ice crystals in three-dimensional space," J. Opt. Soc. Am. A **13,** 2072–2085 (1996).
36. Z. Liao, H. L. Wong, B. Yang, and Y. Yuan, "A transmitting boundary for transient wave analyses," Sci. Sin. **27,** 1063–1076 (1984).
37. P. Yang and K. N. Liou, "An efficient algorithm for truncating spatial domain in modeling lighting scattering by finite-difference technique," J. Comput. Phys. **140,** 346–369 (1998).
38. J. P. Berenger, "A perfectly matched layer for the absorption of electromagnetic waves," J. Comput. Phys. **114,** 185–200 (1994).
39. J. P. Berenger, "Three-dimensional perfectly matched layer for the absorption of electromagnetic waves," J. Comput. Phys. **127,** 363–379 (1996).
40. D. S. Katz, E. T. Thiele, and A. Taflove, "Validation and extension to three dimensions of the Berenger PML absorbing boundary condition for FD-TD meshes," IEEE Microwave Guided Wave Lett. **4,** 268–270 (1994).
41. A. Taflove and M. E. Brodwin, "Numerical solution of steady-state electromagnetic scattering problems using the time-dependent Maxwell's equations," IEEE Trans. Microwave Theory Tech. **MTT-23,** 623–630 (1975).
42. D. M. Sullivan, "A simplified PML for use with the FDTD method," IEEE Microwave Guided Wave Lett. **6,** 97–99 (1996).
43. B. Engquist and A. Majda, "Absorbing boundary conditions for the numerical simulation of waves," Math. Comput. **31,** 629–651 (1971).
44. G. Mur, "Absorbing boundary condition for the finite-difference approximation of the time-domain electromagnetic-field equations," IEEE Trans. Electromagn. Compat. **EMC-23,** 377–382 (1981).
45. A. Bayliss and E. Turkel, "Radiation boundary conditions for wavelike equations," Commun. Pure Appl. Math. **33,** 707–725 (1980).
46. R. L. Higdon, "Absorbing boundary conditions for difference approximations to the multidimensional wave equation," Math. Comput. **47,** 437–459 (1986).
47. S. A. Schelkunoff, *Electromagnetic Waves* (Van Nostrand, New York, 1943).
48. D. E. Merewether, R. Fisher, and F. W. Smith, "On implementing a numeric Huygen's source in a finite difference program to illustrate scattering bodies," IEEE Trans. Nucl. Sci. **NS-27,** 1829–1833 (1980).
49. P. S. Tuminello, E. T. Arakawa, B. N. Khare, J. M. Wrobel, M. R. Querry, and M. E. Milham, "Optical properties of *Bacillus subtilis* spores from 0.2 to 2.5 μm," Appl. Opt. **36,** 2818–2824 (1997).
50. A. J. Heymsfield and C. M. R. Platt, "A parameterization of the particle size spectrum of ice clouds in terms of the ambient temperature and the ice water content," J. Atmos. Sci. **41,** 846–855 (1984).
51. G. N. Plass and G. W. Kattawa, "Radiative transfer in water and ice clouds in the visible and infrared region," Appl. Opt. **10,** 738–749 (1968).
52. W. P. Arnott, Y. Liu, and J. Hallet, "Unreasonable effectiveness of mimicking measured infrared extinction by hexagonal ice crystals with Mie ice spheres," in *Optical Remote Sensing of the Atmosphere*, Vol. 5 of 1997 OSA Technical Digest Series (Optical Society of America, Washington, D.C., 1997), pp. 216–218.
53. D. L. Mitchell, A. Macke, and Y. G. Liu, "Modeling cirrus clouds. Part II: Treatment of radiative properties," J. Atmos. Sci. **53,** 2967–2988 (1996).
54. Z. Sun and K. P. Shine, "Parameterization of ice cloud radiative properties and its application to the potential climatic importance of mixed phase clouds," J. Climate **8,** 1874–1888 (1995).
55. A. Ono, "The shape and riming properties of ice crystals in natural clouds," J. Atmos. Sci. **26,** 138–147 (1969).
56. A. H. Auer, Jr., and D. L. Veal, "The dimension of ice crystals in natural clouds," J. Atmos. Sci. **27,** 919–926 (1970).
57. R. G. Pinnick, S. C. Hill, P. Nachman, G. Videen, G. Chen, and R. K. Chang, "Aerosol fluorescence spectrum analyzer for measurement of single micrometer-sized airborne biological particles," Aerosol. Sci. Technol. **28,** 95–104 (1998).
58. G. Videen, W. B. Sun, and Q. Fu, "Light scattering from irregular tetrahedral aggregates," Opt. Commun. **156,** 5–9 (1998).